Postprint of: Alibakhshi, A., Dastjerdi, Sh., Malikan, M., Eremeyev, VA, Nonlinear free and forced vibrations of a dielectric elastomer-based microcantilever for atomic force microscopy, CONTINUUM MECHANICS AND THERMODYNAMICS, DOI: 10.1007/s00161-022-01098-4

Nonlinear free and forced vibrations of a dielectric elastomer-based microcantilever for atomic force microscopy

Amin Alibakhshi [1], Shahriar Dastjerdi [2], Mohammad Malikan *[3], and Victor A. Eremeyev [3,4]

[1] Department of Mechanical Engineering, Science and Research Branch, Islamic Azad University; alibakhshiamin@yahoo.com

[2] Division of Mechanics, Civil Engineering Department, Akdeniz University, Antalya, Turkey; dastjerdi_shahriar@yahoo.com

[3] Department of Mechanics of Materials and Structures, Faculty of Civil and Environmental Engineering, Gdansk University of Technology, Gdansk, Poland; mohammad.malikan@pg.edu.pl

[4] DICAAR, Università degli Studi di Cagliari, Via Marengo, 2, 09123, Cagliari, Italy; victor.eremeev@pg.edu.pl

* Correspondence: mohammad.malikan@pg.edu.pl, mohammad.malikan@yahoo.com

Abstract

The majority of atomic force microcode (AFM) probes work based on piezoelectric actuation. However, some undesirable phenomena such as creep and hysteresis may appear in the piezoelectric actuators that limit their applications. This paper proposes a novel AFM probe based on dielectric elastomer actuators (DEAs). The DE is modeled via the use of a hyperelastic Cosserat model. Size effects and geometric nonlinearity are included utilizing the modified couple stress theory and the von-Kármán strains. A non-contact interaction condition is adopted for AFM, which is taken into account via the van der Waals force. Governing equations are derived employing Hamilton's principle, and a reduced model is obtained using an extended Galerkin scheme. The free vibration of the system is formulated when a static voltage is applied to the elastomer. The forced vibration is then formulated when the system is under a combination of static and dynamic voltages. The ordinary differential equations of the free and forced vibrations are numerically and analytically solved by the backward differentiation method and multiple time scales method, respectively. Results are presented in time histories, phase portraits, Poincaré maps, fast Fourier transforms, and frequency amplitude curves. Overall, the obtained information displays that the system undergoes quasiperiodic and periodic motions. Moreover, the resonant response of the DE-based AFM is softening-type.

Keywords: Dielectric elastomers-based atomic force microscopy; Electrically actuated atomic force microcopy; Nonlinear vibrations; Nonlinear resonance

1. Introduction

Dielectric elastomers are intelligent hyperelastic structures that belong to electrostrictive polymers [1–4]. They have received considerable critical attention due to their encouraging features such as large deformations, lightweight, flexibility, durability, and compatibility. The main applications of DEs find in soft robotics, where they can be used to work as actuators and sensors [5, 6]. In addition to these applications, they can also operate as energy harvesters and resonators [7–9].

Various types of structures, including balloons, square, circular, and rectangular membranes, tubes and cylinders, beams in different scales have been proposed to design dielectric elastomer (DE)-based structures. The past two decades have witnessed a large growth in the dynamic modeling of DEs based on the above-stated structures. In what follows, a detailed review is provided on these dynamic modeling. Zhu et al. [10] analyzed nonlinear vibrations of a balloon excited by a DE actuator. Random vibrations of a DE-based balloon were studied by Jin and Huang [11]. DC dynamic instabilities of a balloon shape DE were identified by Sharma et al. [12], who utilized an energy approach in their research. Linear and nonlinear dynamics of a circular DE with particular attention to the strain-stiffening of elastomers were researched by Wang and co-researchers [13]. Alibakhshi and Heidari [14] proposed an analytical method, i.e., the multiple scales method for solving nonlinear vibrations of DE balloons. The same authors [15] analyzed the chaos in a DE balloon by considering the influence of the second strain invariant. Zhang and Chen [16] explored the influence of geometry sizes on beating vibrations of a square and rectangular DE membrane. Heidari et al. [17] discussed chaotic domains in a DE elastomer membrane. Alibakhshi and co-workers [18] analyzed static and dynamical instabilities together with nonlinear resonances of a DE rectangular membrane by employing different hyperelastic models. Vibrations of a resonator based on DE microbeams were studied by Feng et al. [19]. Feng and co-workers [20] analyzed large amplitude vibrations of a DE microbeam resonator. Alibakhshi and co-researcher [21] investigated the nonlinear dynamics of a DE microbeam considering geometrical and physical nonlinearities. A closer look at the above review reveals that systems based on DE reveal rich dynamical behaviors. In the time domain, they encounter diverse routes to chaos such as quasiperiodicity, chaos. Furthermore, in the frequency domain, softening and hardening resonant behaviors, jump, and hysteresis emerge in DEs. The resonant frequency of devices based on DEs can be controlled easily after fabrication which is a notable advantage of DEs. In some views, DEs can induce large amplitude vibrations that can be used as resonators, and in some cases, they possess damping and thereby can be used as electromechanical dampers.

In the laboratory, different instruments are utilized for probing and imaging too small objects. For instance, microscope, telescope, camera, scanning tunneling microscopy (STM), scanning probe electrochemistry (SPE), atomic force microscopy (AFM), etc. Researchers have shown an increased interest in using AFM due to maneuverability and applicability. AFM finds many applications such as surface probing, surface manipulation, biological research, force measurement, and so on.

A common architecture of AFM involves a microcantilever with a tip apex. By actuating the microcantilever, the tip apex touches and probes the intended surface [22–24]. In the most theoretical and experimental studies on AFMs piezoelectric actuation-based microcantilevers have been utilized. In general, although piezoelectric actuation works efficiently in many environments and applications, some limitations have been reported. For example, the piezoelectric actuation may cause spurious peaks in the frequency response spectrum, which is not observed in the cantilever resonance. Moreover, creep and hysteresis may appear in piezoelectric actuation. Another drawback of AFM based on piezoelectric actuation is slow scanning, that is, the slow scanning speed. These limitations have an undesirable effect on the performance of AFM. An alternative to piezoelectric actuation is electrostatic actuation. For this reason, electrostatic actuation may discard the above-stated limitations [25, 26].

This paper aims to propose an innovative electrostatic actuation based on dielectric elastomers, which have shown their applicability in MEMS. They can easily tune their resonant frequency after fabrication and can be designed in different shapes to have the best performance. DE actuators also have a fast speed actuation that discards the speed limitation in piezoelectric actuation. With developments in micro and nanofabrication and due to the capacity of DEs to operate effectively in macro and nanoscales, this paper proposes AFM based on DE actuators. There is not a clearly presented study on AFM based on DEs. In this paper, a non-contact dynamic model for dielectric elastomer-atomic force microscopy is developed based

on hyperelastic micropolar mechanics. (DE-AFM). Dynamic equations of motion are acquired and solved numerically and analytically based on an energy approach. Then, numerical results are discussed in detail.

2. Theory and Formulation

The schematic figure of the dielectric elastomer atomic force microscopy (DE-AFM) is depicted in Fig. 1. The DE-AFM consists of a DE microcantilever, which its free end contacts the surface of an arbitrary sample. The DE microcantilever is of length L, width b, and thickness d, which its bottom and upper surfaces are coated with compliant electrodes. The microcantilever is placed on a base substrate. By applying an electrical load to the electrodes through a conductive wire, the DE actuator is activated, and the cantilever vibrates with evolving time coordinate t, and its tip probes the surface of the sample. When the applied voltage is connected to electrodes directly attached to the top and bottom surfaces of the elastomer, the electrodes gain opposite electrical charges. Microcantilevers in AFM deforms and deflects by an attractive force between these charges. When the microcantilever oscillates and experiences deflection, the lower electrode may come near the base structure, and the microbeam collapses. An electrode is located on the base structure and connects to the facing electrode to avoid this levitation effect. This causes these electrodes to have similar charges and repel each other [27].

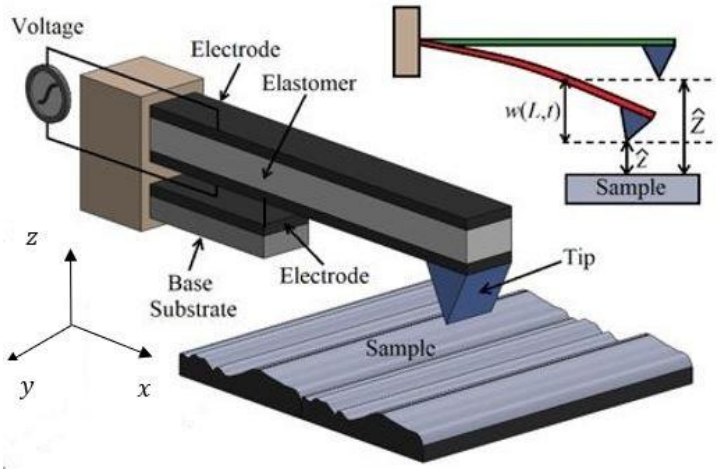

Figure. 1. Schematic view of a dielectric elastomer atomic force microscopy.

2.1 Displacement field

The deformation of the DE microcantilever is modeled on the basis of the Euler-Bernoulli beam theory, which is formulated as [28, 29]

$$U_x(x,z,t) = -z\frac{\partial w(x,t)}{\partial x}$$

$$U_y(x,y,t) = 0$$

$$U_z(x,y,t) = w(x,t) \tag{1}$$

in which U_x, U_y, and U_z are displacements components along with x, y, z coordinates.

It is noted that the deformation behavior of the Euler-Bernoulli beam model in this paper is based on the nonlinear strains and the extensibility of the centerline is neglected. In the beam model considered here, the effect of shear deformation and rotary inertia has been ignored. All the nonlinear terms in this paper are related to the geometric nonlinearity inside the strain energy only. However, more sophisticated models accounting for the shear deformation and rotary inertia can also be used for the system [30–35].

To complete the dynamic modeling of the system, the potential energy, the kinetic energy, and the damping force are formulated in the following, respectively. Then, employing Hamilton's principle, the partial differential equation (PDE) will be derived and decomposed via a single-mode Galerkin technique [36].

2.2 Potential Energy

The strain energy of the elastomer, the potential of the tip-sample interaction, size effects, and the potential of electrical load constitute the total potential energy of the DE-AFM, which are formulated in the following.

The elastomer in the microcantilever follows finite deformation. For this reason, a nonlinear model should be adopted to obtain its strain energy. Therefore, a hyperelastic Cosserat model developed by Reddy and Srinivasa is utilized, in which moderate rotation, finite deformation, and size effect are involved. The hyperelastic Cosserat model in line with the Euler-Bernoulli is formulated as [37, 38]

$$U_{HC} = \int_{\mathcal{V}} \frac{1}{2}\left[a_1 E_{xx}^2 + a_2 E_{zz}^2 + a_3 \left(\frac{\partial^2 w}{\partial x^2}\right)^2 + 2a_4 E_{xx} E_{zz}\right] d\mathcal{V} \tag{2}$$

in which $\mathcal{V}$ is the occupied volume by DE; E_{xx} and E_{zz} are axial and transverse components of Green-Lagrange strain tensor, respectively, which are defined below [39]

$$E_{xx} = \frac{1}{2}\left(\frac{\partial w}{\partial x}\right)^2 - z\frac{\partial^2 w}{\partial x^2}$$

$$E_{zz} = \frac{1}{2}\left(\frac{\partial \mathrm{w}}{\partial \mathrm{x}}\right)^2 \tag{3}$$

In Eq. (2), a_1, a_2, and a_4 stand for elastic constants, and a_3 is a size effect parameter. These parameters will be defined in the following. It is mentioned that the size effect in this hyperelastic model is based on the modified couple stress theory. It is mentioned that classical hyperelastic models such as neo-Hookean and Mooney-Rivlin can also be used for the system.

Substituting Eq. (3) into Eq. (2), the potential of elastic energy is acquired as

$$U_{HC} = \int_0^L \left[\frac{1}{8}a_1 A\left(\frac{\partial w}{\partial x}\right)^4 + \frac{1}{8}a_2 A\left(\frac{\partial w}{\partial x}\right)^4 + \frac{1}{4}a_4 A\left(\frac{\partial w}{\partial x}\right)^4 + \frac{1}{2}a_1 I\left(\frac{\partial^2 w}{\partial x^2}\right)^2 + \frac{1}{2}a_3\left(\frac{\partial^2 w}{\partial x^2}\right)^2\right] dx \tag{4}$$

in which $I = bd^3/12$ is the second moment of cross-section; the cross-section area is denoted by $A = bd$. The elastic constants and the length scales parameter are expressed as [40]

$$a_1 = a_2 = 2\mu + \lambda,\ a_4 = \lambda,\ a_3 = 2\mu\ell^2 \tag{5}$$

In the above equation, μ is the shear modulus, λ stands for the second Lame's modulus, and ℓ denotes the internal length scale parameter. The elastic constants, i.e., μ and λ are defined based on the assumption of incompressibility condition in DE, which results in

$$\mu = \frac{E}{3},\ \lambda = 50\mu,\ \nu = \frac{\lambda}{2(\lambda+\mu)} \approx 0.49 \tag{6}$$

Combining Eqs. (4), (5), and (6), the elastic energy is rewritten as

$$U_{HC} = \int_0^L \left[\frac{51\mu A}{2}\left(\frac{\partial w}{\partial x}\right)^4 + \mu A\ell^2\left(\frac{\partial^2 w}{\partial x^2}\right)^2 + 26\mu I\left(\frac{\partial^2 w}{\partial x^2}\right)^2\right] dx \tag{7}$$

The electrical load makes a potential in the system, which is defined as [9, 21]

$$U_{EL} = \int_0^L \left[-\frac{1}{2}\epsilon_0 A\left(\frac{\Phi}{d}\right)^2\left(\frac{\partial w}{\partial x}\right)^2\right] dx \tag{8}$$

where ϵ_0 indicates the electrical permittivity of the elastomer.

It is assumed that the system works in a vacuum environment. Based on this assumption, the van der Waals non-contact force is utilized to incorporate the potential of the tip-sample interaction, namely [41]

$$F_{vdW} = -\frac{HR}{6\hat{z}^2} \tag{9}$$

In the above equation, H is the Hamaker constant, R is the radius of the spherical tip apex, and $\hat{z}$ stands for instantaneous tip/sample separation, which is defined as

$$\hat{z} = \hat{Z} - w(L,t) \tag{10}$$

in which $\hat{Z}$ shows the initial tip/sample separation distance.

The potential of the tip/sample interaction based on Eq. (9) is expressed as [42]

$$U_{TIP} = \int F_{vdW}\ d\hat{z} = -\frac{HR}{6[Z-w(L,t)]} \tag{11}$$

Then, the final value of the potential energy of the DE-AFM can be obtained below

$$U_S = \left\{\int_0^L \left[\frac{51\mu A}{2}\left(\frac{\partial w}{\partial x}\right)^4 + \mu A\ell^2\left(\frac{\partial^2 w}{\partial x^2}\right)^2 + 26\mu I\left(\frac{\partial^2 w}{\partial x^2}\right)^2\right] dx\right\} + \left\{\int_0^L \left[-\frac{1}{2}\epsilon_0 A\left(\frac{\Phi}{d}\right)^2\left(\frac{\partial w}{\partial x}\right)^2\right] dx\right\} + \left\{-\frac{HR}{6[Z-w(L,t)]}\right\} \tag{12}$$

2.3 Kinetic Energy

The kinetic energy due to the motion of the microcantilever is acquired as [43]

$$U_K = \frac{1}{2}\rho A\int_0^L \left(\frac{\partial w}{\partial t}\right)^2 dx \tag{13}$$

in which ρ is the mass-density of the DE.

2.4 Damping Force

Dielectric elastomers may possess viscous damping. Therefore, the influence of viscous damping on the DE-AFM will be analyzed. The damping effect in the system is incorporated by introducing its work as the following

$$\delta W_D = -c_d\int_0^L \frac{\partial w}{\partial t}\delta w dx \tag{14}$$

In the above equation c_d is the damping coefficient.

2.5 Hamilton's Principle

Governing equations for mechanical structures can be derived from different techniques such as the Lagrangian method, Hamilton's method, etc. [44–50]. The governing equation and corresponding boundary conditions are derived through the use of the Hamilton's principle, which states

$$\int_{t_1}^{t_2} \delta[U_K - U_S]\, dt + \int_{t_1}^{t_2} \delta W_D\, dt = 0 \tag{15}$$

Substituting Eqs. (12), (13), and (14) into Eq. (15), the PDE governing the motion of the DE-AFM and the corresponding boundary conditions are, respectively, derived as

$$\rho A \frac{\partial^2 w}{\partial t^2} + c_d \frac{\partial w}{\partial t} + 52\mu I \frac{\partial^4 w}{\partial x^4} + 2\mu A \ell^2 \frac{\partial^4 w}{\partial x^4} - 306\mu A \frac{\partial^2 w}{\partial x^2} \left(\frac{\partial w}{\partial x}\right)^2 + \epsilon_0 A \left(\frac{\Phi}{d}\right)^2 \frac{\partial^2 w}{\partial x^2} = 0 \tag{16}$$

in which the boundary conditions are

$$w(0,t) = 0,\ \frac{\partial w}{\partial x}(0,t) = 0,\ \frac{\partial^2 w}{\partial x^2}(L,t) = 0$$

$$52\mu I \frac{\partial^3 w}{\partial x^3}(L,t) + 2\mu A \ell^2 \frac{\partial^3 w}{\partial x^3}(L,t) = -\frac{HR}{6[Z - w(L,t)]^2} \tag{17}$$

2.6 Nondimensionalization

The governing equation and boundary conditions, i.e., Eqs. (16) and (17) are made dimensionless in order for the numerical calculation to become straightforward. For this purpose, the following dimensionless quantities are introduced

$$x^* = \frac{x}{L}, w^* = \frac{w}{L}, t^* = t\sqrt{\frac{\mu I}{\rho A L^4}}, c = \frac{c_d L^4}{\mu I}\sqrt{\frac{\mu I}{\rho A L^4}}, \eta_1 = 52, \eta_2 = \frac{2\mu A \ell^2}{\mu I}$$

$$\beta_1 = \frac{306\mu A L^2}{\mu\, I}, \beta_2 = \frac{AL^2}{I}, V = \frac{\epsilon_0}{\mu}\left(\frac{\Phi}{d}\right)^2, Z^* = \frac{\hat{Z}}{L}, \eta_3 = \frac{HR}{6\mu I} \tag{18}$$

Substituting Eq. (18) into Eqs. (16) and (17), a dimensionless form of the equation of motion and the boundary conditions are derived as (asterisk symbol is omitted for convenience)

$$\frac{\partial^2 w}{\partial t^2} + c\frac{\partial w}{\partial t} + (\eta_1 + \eta_2)\frac{\partial^4 w}{\partial x^4} - \beta_1 \frac{\partial^2 w}{\partial x^2}\left(\frac{\partial w}{\partial x}\right)^2 + \beta_2 V \frac{\partial^2 w}{\partial x^2} = 0 \tag{19}$$

with

$$w(0,t) = 0,\ \frac{\partial w}{\partial x}(0,t) = 0,\ \frac{\partial^2 w}{\partial x^2}(1,t) = 0,\ (\eta_1 + \eta_2)\frac{\partial^3 w}{\partial x^3}(1,t) = -\frac{\eta_3}{[Z - w(1,t)]^2} \tag{20}$$

2.7 Extended Galerkin Scheme

Eq. (19) is a PDE with time-dependent boundary conditions. An extended Galerkin discretization method is applied to transform this PDE to an ordinary differential equation (ODE). The extended Galerkin method is started by introducing a new variable as [51]

$$w(x,t) = q(x,t) + f(t)g(x) \tag{21}$$

in which $f(t)$ is defined as

$$f(t) = -\frac{\eta_3}{(\eta_1+\eta_2)[Z-w(1,t)]^2} \tag{22}$$

In Eq. (21), $g(x)$ is an arbitrary function. In the present paper, this function is expressed as

$$g(x) = -\frac{1}{6}x^2 + \frac{1}{2}x^3 - \frac{1}{2}x^4 + \frac{1}{6}x^5 \tag{23}$$

where function $g(x)$ satisfies the following conditions

$$g(0) = \frac{dg}{dx}(0) = g(1) = \frac{dg}{dx}(1) = \frac{d^2g}{dx^2}(1) = 0, \quad \frac{d^3g}{dx^3}(1) = 1 \tag{24}$$

Substituting Eq. (21) into Eq. (19), a new PDE in terms of $q(x,t)$ is derived, which have homogeneous boundary conditions as

$$q(0,t) = 0, \ \frac{\partial q}{\partial x}(0,t) = 0, \ \frac{\partial^2 q}{\partial x^2}(1,t) = 0, \ \frac{\partial^3 q}{\partial x^3}(1,t) = 0 \tag{25}$$

By applying the extended Galerkin scheme and using the separation-of-variable approach, we write

$$q(x,t) = \phi(x)W(t) \tag{26}$$

where $W(t)$ stands for the time-depended generalized coordinate; $\phi(x)$ denotes the eigenfunction for a cantilever beam. It is noted that a single-mode vibration is considered in this work.

$$\ddot{W} + c\dot{W} + Y_2W + Y_1\ddot{f} + cY_1\dot{f} + Y_3f + Y_4f^3 + Y_5f^2W + Y_6f^2W + Y_7fW^2 + Y_8fW^2 + Y_9W^3 + Y_{10}VW + Y_{11}Vf(t) = 0 \tag{27}$$

in which

$$Y_1 = \int_0^1 [g(x)\phi(x)]\,dx\,, \qquad Y_2 = \int_0^1 \left[(\eta_1+\eta_2)\phi(x)\phi^{(4)}(x)\right]dx$$

$$Y_3 = \int_0^1 \left[(\eta_1+\eta_2)g^{(4)}(x)\phi(x)\right]dx\,, \qquad Y_4 = -\int_0^1 [\beta_1\phi(x)g'(x)^2g''(x)]\,dx$$

$$Y_5 = -\int_0^1 [2\beta_1\phi(x)g'(x)g''(x)\phi'(x)]\,dx \qquad Y_6 = -\int_0^1 [\beta_1\phi(x)g'(x)^2\phi''(x)]dx$$

$$Y_7 = -\int_0^1 [\beta_1\phi(x)g''(x)\phi'(x)^2]\,dx \qquad Y_8 = -\int_0^1 [2\beta_1\phi(x)g'(x)\phi'(x)\phi''(x)]\,dx$$

$$Y_9 = \int_0^1 [-\beta_1\phi(x)\phi'(x)^2\phi''(x)]\,dx\,, \qquad Y_{10} = \int_0^1 [\beta_2\phi(x)\phi''(x)]\,dx$$

$$Y_{11} = \int_0^1 [\beta_2 \phi(x) g''(x)]\, dx \tag{28}$$

In the above equations, the dot symbol stands for derivatives with respect to the dimensionless time coordinate, and the prime symbol indicates derivative with respect to the dimensionless axial coordinate. In the following, the equation of motion, i.e., Eq. (27), is solved numerically and analytically. Then, results based on these solutions are compared to examine the accuracy of the proposed methods.

3. Solution method

In this section, the governing equation is solved analytically using the multiple time scales method. The ordinary differential equation, i.e., Eq. (27), contains the function $f(t)$, Eq. (22), which includes a fractional term of the generalized coordinate. We expand this function using the Taylor series to convert the ODE into a general form, namely

$$M\,\ddot{W} + C\dot{W} + K\,W + K_{nq}W^2 + K_{nc}W^3 = \text{External force} \tag{29}$$

where M stands for the mass, C stands for the damping, K refers to linear term; K_{nc} is a term related to the quadratic nonlinearity; K_{nq} is cubic nonlinear term; "External force" shows term(s) related to external excitation of the system, which takes different forms depending on the problem.

Function $f(t)$ is expanded to a first-order approximation as follows

$$f(t) = -\frac{\eta_3}{(\eta_1+\eta_2)[Z-w(1,t)]^2} = A + BW(t) \tag{30}$$

in which

$$A = -\frac{\eta_3}{Z^2(\eta_1+\eta_2)},\ B = -\frac{2(\eta_3\phi(1))}{Z^3(\eta_1+\eta_2)} \tag{31}$$

Substituting Eq. (30) into Eq. (27), we get the general form of the ODE as

$$M\,\ddot{W} + C\dot{W} + K\,W + K_{nq}W^2 + K_{nc}W^3 + \Gamma W + K_1 = 0 \tag{32}$$

in which

$$M = 1 + BY_1, \qquad C = c + cBY_1$$

$$K = Y_2 + BY_3 + 3A^2BY_4 + A^2Y_5 + A^2Y_6 \qquad K_{nq} = 3AB^2Y_4 + 2ABY_5 + 2ABY_6 + AY_7 + AY_8$$

$$K_{nc} = B^3Y_4 + B^2Y_5 + B^2Y_6 + BY_7 + BY_8 + Y_9 \qquad \Gamma = VY_{10} + BVY_{11}$$

$$K_1 = AVY_{11} \tag{33}$$

4. Free vibration analysis

The free vibration of the DE-based AFM can be formulated when the applied voltage is a DC polarization voltage, such that

$$V = V_{DC} = \frac{\epsilon_0}{\mu}\left(\frac{\Phi_{dc}}{d}\right)^2 \tag{34}$$

where Φ_{dc} is a DC voltage.

Substituting Eq. (34) into Eq. (27), the free vibration ODE is derived as

$$\ddot{W} + c\dot{W} + Y_2 W + Y_1 \ddot{f} + cY_1 \dot{f} + Y_3 f + Y_4 f^3 + Y_5 f^2 W + Y_6 f^2 W + Y_7 f W^2 + Y_8 f W^2 + Y_9 W^3 + Y_{10} V_{DC} W + Y_{11} V_{DC} f(t) = 0 \quad (35)$$

4.1 Analytical solutions of free vibration

If the applied voltage to the elastomer is a DC polarization voltage, the system undergoes a free vibration. For this purpose, we consider $V = V_{DC}$. Thus, Eq. (32) is transformed into the following form

$$M\ddot{W} + C\dot{W} + (K + \Gamma_1) W + K_{nq} W^2 + K_{nc} W^3 = 0 \quad (36)$$

where $\Gamma_1 = V_{DC} Y_{10} + B V_{DC} Y_{11}$.

Eq. (36) is divided by M, which leads to

$$\ddot{W} + \bar{C}\dot{W} + \omega_0^2 W + \alpha_q W^2 + \alpha_c W^3 = 0 \quad (37)$$

where $\bar{C} = C/M$, $\omega_0^2 = (K + \Gamma_1)/M$, $\alpha_q = K_{nq}/M$, and $\alpha_c = K_{nc}/M$.

For the analytical solution of the free vibration, the damping is neglected for simplification. Based on the multiple time-scales method, the approximation solution to Eq. (37) with neglecting the damping is obtained as [52, 53] (it is noted that the details of analytical solutions have not been given in this paper)

$$W = a_0 \cos(\omega t + \beta_0) + \frac{a_0^2 \alpha_q}{6\omega_0^2} [\cos(2\omega t + 2\beta_0) - 3] \quad (38)$$

where a_0 and β_0 are constants showing the amplitude and phase, which are chosen based on the initial condition. The frequency of the free vibration is as follows

$$\omega = \omega_0 \left[1 + \left(\frac{9\omega_0^2 \alpha_c - 10{\alpha_q}^2}{24{\omega_0}^4}\right) a_0^2\right] \quad (39)$$

Here, the free vibration results of the DE-based AFM are presented. Material and geometrical properties are chosen from the previous studies [19, 20, 41, 54]. The length $L = 60\mu$m, width $b = 10\mu$m, thickness $d = 0.65\mu$m, Hamaker constant $H = 2.96 \times 10^{-19}$J, tip radius $R = 10 \times 10^{-9}$m, shear modulus $\mu = 1$GPa, electrical permittivity $\epsilon_0 = 17.7 \times 10^{-12}$Fm^{-1}, reference tip/sample distance $\hat{Z} = 60$nm. There is limited evidence for the internal length scale parameter of DEs. Hence it is selected as $\ell = 0.02L$. Within this section, the initial velocity for the time integration is equal to $\dot{W}(0) = 0$. The above-stated parameters are utilized in all numerical and analytical solutions unless otherwise stated.

Numerical results are presented for Eq. (35), where a numerical scheme, namely backward differentiation formula, is used to solve it. Analytical solutions of the multiple time scales method are expressed for Eq. (38).

In Fig. 2, the results of the numerical and analytical methods are compared to examine the accuracy and reliability of our results. In this figure, $\Phi_{dc} = 100$Volt, damping is $c = 0$, and the initial conditions are $W(0) = 0.0001$. Moreover, the constants in Eq. (38) for the analytical solutions are $a_0 = 0.0001$ and $\beta_0 = 0$.

From Fig. 2, we see a perfect agreement between the numerical and analytical methods. This means that the simplification process in Section. 3 (Solution method) is correct. Therefore, we can also adopt such a simplification for the forced vibration of the system, which will be conducted in the next sections. The

free vibration can be explored either analytically or numerically in the following. We use the numerical method in this subsection to analyze the influence of the system's parameters on the free vibration.

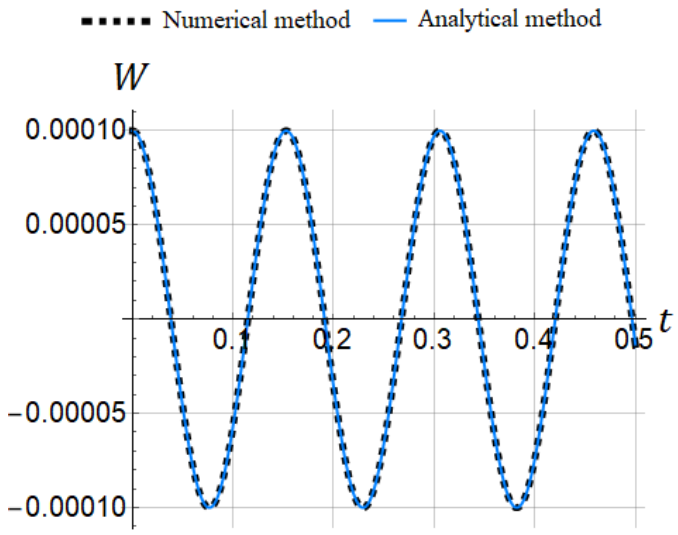

Figure. 2. Free vibration of the dielectric elastomer-based microcantilever atomic force microscope probe. A comparison between numerical and analytical methods.

In Fig. 3, we identify the general response of the system under a static voltage (free vibration of the system). In this figure, a time-integration is carried out to 10 dimensionless time-coordinate. Then, the time history and phase-plane diagram are depicted to identify the dynamic response. The system's parameters and initial deflections are chosen as $\Phi_{dc} = 100\text{Volt}$, $c = 0$ and $W(0) = 0.0001$. In response to a static voltage, a periodic and regular vibration is elicited from this figure. The presence of a closed curve in the phase-plane diagram and predictable motions in the time history is evidence for the periodicity of DE-based AFM.

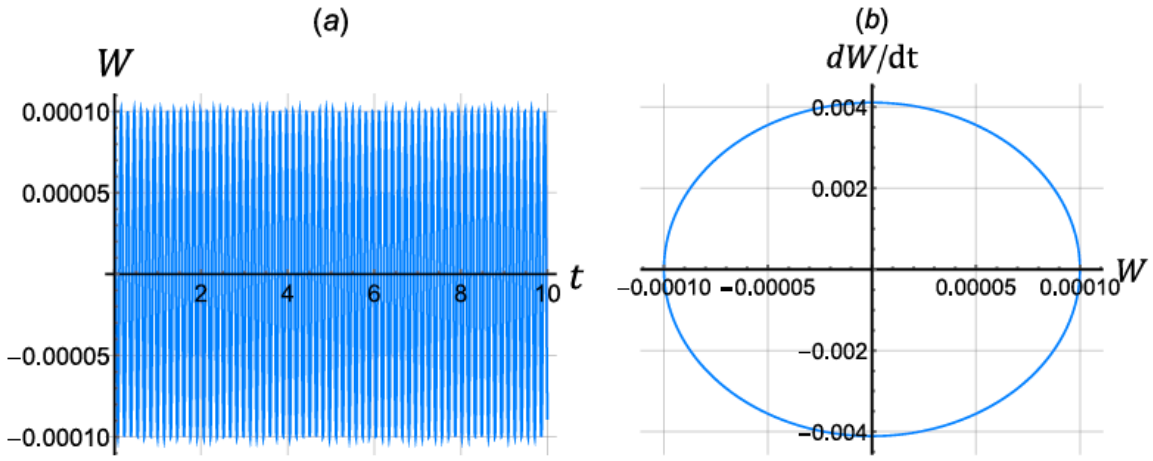

Figure. 3. Free vibration of the dielectric elastomer-based microcantilever atomic force microscope probe under $\Phi_{dc} = 100\text{Volt}$, and $c = 0$ with $W_0 = 0.0001$. (a) time history, (b) phase-plane diagram.

It is by now generally have seen that elastomeric materials have viscosity, which may significantly affect the response of DEs. To analyze how the viscous damping force can affect the free vibration response of DE-based AFM, Fig. 4 is depicted. The DC polarization voltage takes the value of $\Phi_{dc} = 100\text{Volt}$, and the damping coefficient is $c = 0.1$. A decreasing trend of the response amplitude is observed by considering the damping in DE-based AFM. With changing the time, viscosity decreases the response amplitude and dissipates energy in the system. We speculate that this dissipation process might decrease the performance of DE-based AFM, where high-amplitude vibrations for image propping are required.

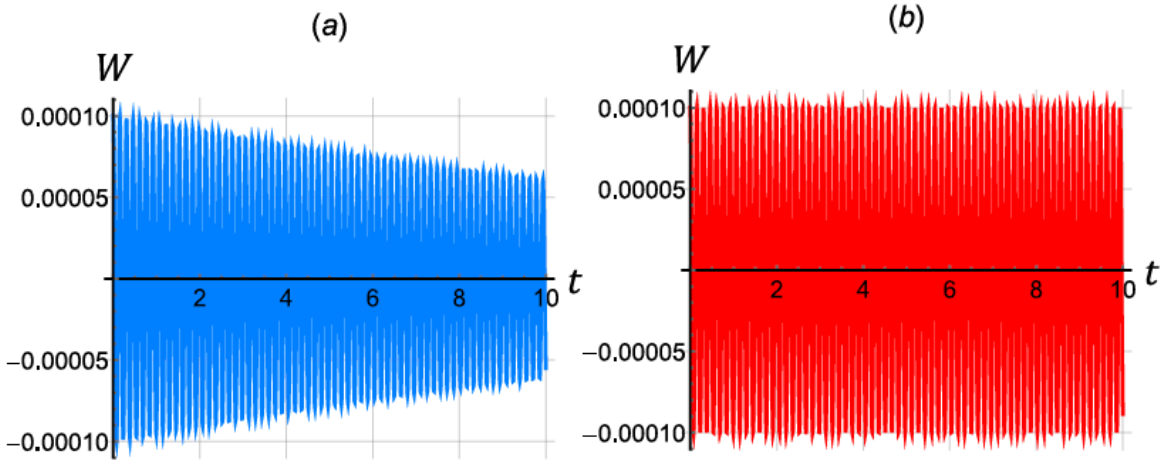

Figure. 4. Influence of the damping on the free vibration of the dielectric elastomer-based microcantilever atomic force microscope probe under $\Phi_{dc} = 100\text{Volt}$ with $W(0) = 0.0001$. (a) time history for and $c = 0.1$, (b) time history for and $c = 0$.

5. Frequency analysis of the free vibration

In this section, the frequency of the free vibration is analyzed, i.e., solution of Eq. (39). It is noted that this frequency can reveal the hardening and softening response in the system. Regardless of the sign, the presence of the quadratic nonlinearity α_q in Eq. (39) indicates a softening response, that is, decreasing the frequency of the free vibration ω. By contracts, the sign of the cubic nonlinearity α_c plays an important role in defining the softening and hardening in terms of ω. Using the material and geometrical parameters in the previous section and $\Phi_{dc} = 100\text{Volt}$ and $c = 0$, the frequency of the free vibration versus the parameter a_0 is depicted in Fig. 5. We see in Fig. 5 that the frequency decreases that is due to the presence of the $\alpha_q = 0.0441058$ and $\alpha_c = -1.34858 \times 10^8$. This output exhibits the softening response of the DE-based AFM, which is consistent with conventional AFMs where linear materials and piezoelectric actuation are utilized.

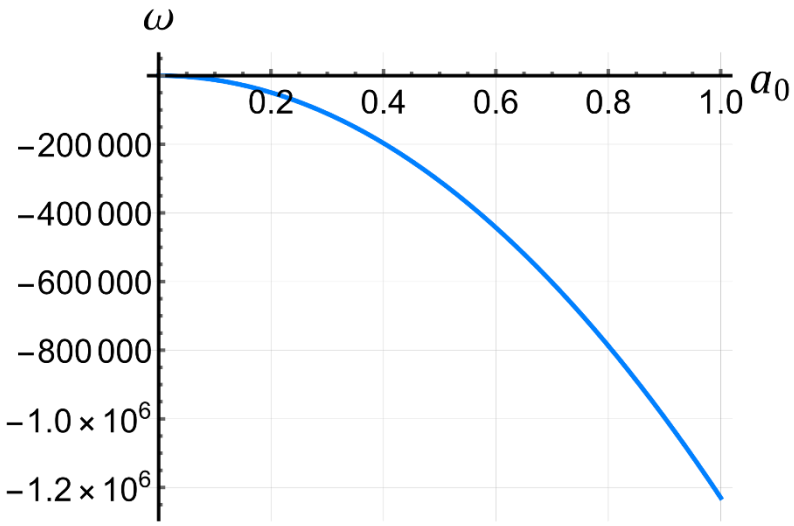

Figure. 5. Frequency of the free vibration of the dielectric elastomer-based microcantilever atomic force microscope probe showing the softening response.

6. Forced vibration analysis

If the voltage varies with time, the forced vibration of the DE-based microcantilever arises. Complexity arises in DEs upon application of a time-dependent electrical load. Time-dependency of voltage makes nonlinear dynamics of DE, which are of importance to be analyzed. The dynamic equation of the system is obtained by using the following equation

$$V = V_{DC}[1 + V_{AC}\cos(\Omega t)]^2 \tag{40}$$

where

$$V_{DC} = \frac{\epsilon_0}{\mu}\left(\frac{\Phi_{dc}}{d}\right)^2, V_{AC} = \frac{\Phi_{ac}}{\Phi_{dc}}, \Omega = \widehat{\omega}\sqrt{\frac{\rho A L^4}{\mu I}} \tag{41}$$

in which Ω is dimensionless excitation frequency; Φ_{ac} indicate the amplitude of AC voltage.

Inserting Eq. (41) into Eq. (27), the dynamic equation is expressed as

$$\ddot{W} + c\dot{W} + Y_2 W + Y_1 \ddot{f} + cY_1 \dot{f} + Y_3 f + Y_4 f^3 + Y_5 f^2 W + Y_6 f^2 W + Y_7 f W^2 + Y_8 f W^2 + Y_9 W^3 + Y_{10}[V_{DC}(1 + V_{AC}\cos(\Omega t))^2]W + Y_{11}[V_{DC}(1 + V_{AC}\cos(\Omega t))^2] f(t) = 0 \quad (42)$$

6.1 Analytical solutions of forced vibration

In this section, we solve the forced vibration of the system analytically using the multiple time-scale method. The main purpose is to obtain a closed-form of the frequency-amplitude equation for analyzing the nonlinear resonance of the system.

The dynamic voltage expressed in Eq. (40) is expanded, such that

$$V = V_{DC}[1 + V_{AC}\cos(\Omega t)]^2 = V_{DC} + V_{DC}V_{AC}^2 \cos^2(\Omega\, t) + 2V_{Dc}V_{AC}\cos(\Omega t) \quad (43)$$

It is assumed the V_{AC} is much smaller than V_{DC}, thereby the terms containing V_{AC}^2 in Eq. (43) is neglected. Substituting Eq. (43) into Eqs. (32) and (33), we get

$$M\,\ddot{W} + C\dot{W} + (K + \Gamma_1)W + K_{nq}W^2 + K_{nc}W^3 = \bar{F}_1\cos(\Omega t) + (\bar{F}_2 + \bar{F}_3)\cos(\Omega t)\,W \quad (44)$$

where $\Gamma_1 = V_{DC}Y_{10} + BV_{DC}Y_{11}$; $\bar{F}_1 = -2V_{DC}V_{AC}Y_{11}A$; $\bar{F}_2 = -2V_{DC}V_{AC}Y_{10}$; $\bar{F}_3 = -2V_{DC}V_{AC}Y_{11}B$.

Similar to the free vibration, Eq. (36) is divided by M, which leads to

$$\ddot{W} + \bar{C}\dot{W} + \omega_0^2\, W + \alpha_q W^2 + \alpha_c W^3 = \bar{F}_1\cos(\Omega t) + (\bar{F}_2 + \bar{F}_3)\cos(\Omega t)\,W \quad (45)$$

where $\bar{C} = C/M$, $\omega_0^2 = (K + \Gamma_1)/M$, $\alpha_q = K_{nq}/M$, $\alpha_c = K_{nc}/M$, $F_1 = \bar{F}_1/M$, $F_2 = \bar{F}_2/M$, and $F_3 = \bar{F}_3/M$.

The frequency-amplitude equation derived using the multiple scale method to the Eq. (45) for a primary resonance is expressed as [55]

$$\left[\bar{C}^2 + \left(\sigma - \frac{9\alpha_q\omega_0^2 - 10\alpha_q^2}{24\omega_0^3}a^2\right)^2\right]a^2 = \left[\frac{F_1}{2\omega_0}\right]^2 \quad (46)$$

where σ is a detuning parameter that for the primary resonance in this paper is given as $\Omega = \omega_0$.

Herein, the results of the frequency-amplitude equation, Eq. (46), are depicted. The material and geometrical parameters are similar to the free vibration. Illustrated in Fig. 6 is the influence of the damping on the frequency response of the DE-based AFM. The DC voltage is $\Phi_{dc} = 100$ Volt and $\Phi_{ac} = 20$ Volt. What stands out from this figure is that the damping decreases the response amplitude significantly when $\bar{C} = 0.1$. Besides, the damping linearizes the resonant trend of the DE-based AFM. Another output of Fig. 6 is that the response is softening-type nonlinearity for ideal DEs, namely a DE without viscous damping. It is noted that the softening response has also been observed in Fig. 5. It is seen that in Fig. 6 (a), two solution branches (upper and lower branches) are very close to each other. Based on Fig. 6, the AFM undergoes multi-valued solutions; as a result of that, the system shows a jump phenomenon and instability. While with the inclusion of the damping, the undesirable jump and instability disappear.

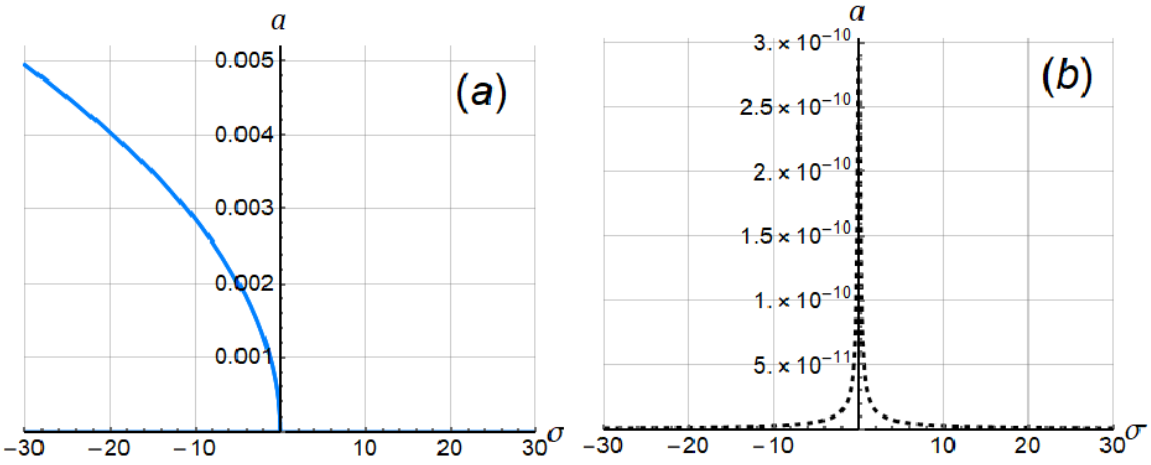

Figure. 6. Frequency amplitude curve of the dielectric elastomer-based microcantilever atomic force microscope probe. (a) $\bar{C} = 0$, (b) $\bar{C} = 0.1$.

The influence of DC voltage Φ_{dc} on the frequency response of the system is studied in Fig. 7. The AC voltage amplitude is small in comparison to the DC voltage, namely $\Phi_{ac} = 20$ Volt. From Fig. 7, we conclude that the response amplitude increases with the increase of the DC voltage. Plus, increasing the DC voltage makes softening resonant behavior weaker. Another finding is that even for a high value of the DC voltage, the damping can reduce the response amplitude and can stabilize the dynamic response of the DE-based cantilever AFM.

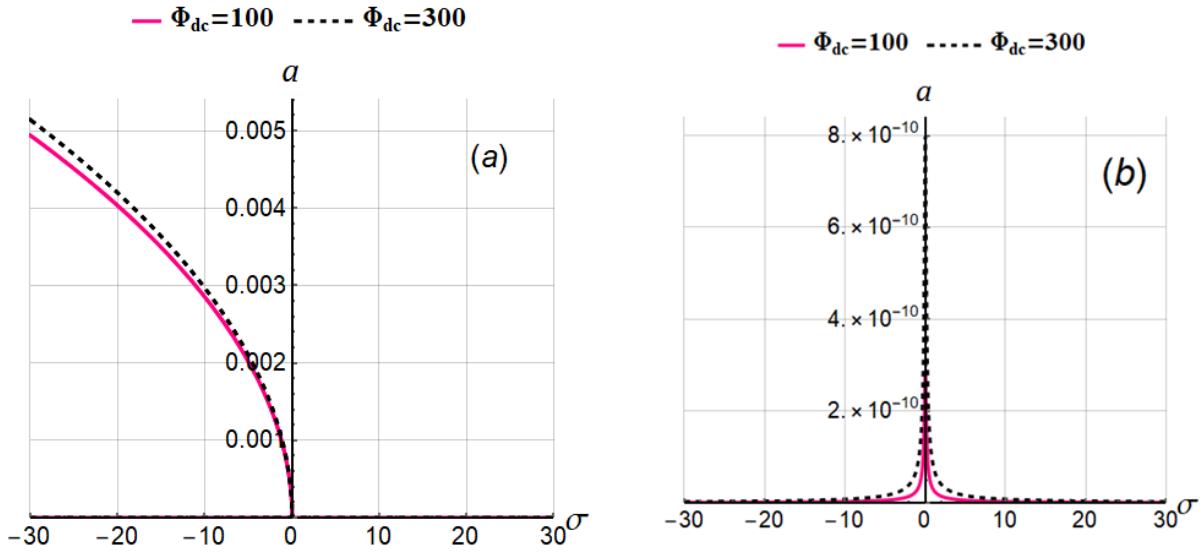

Figure. 7. Influence of DC voltage Φ_{dc} on the Frequency amplitude curve of the dielectric elastomer-based microcantilever atomic force microscope probe. (a) $\bar{C} = 0$, (b) $\bar{C} = 0.1$.

We explore the influence of the AC voltage amplitude on the resonance of the AFM in Fig. 8 when $\Phi_{dc} = 100$. We observed that the AC voltage amplitude does not significantly affect the softening response of the system when the damping is not present in the model. As the figure tells, in a damped DE-based AFM, the amplitude of the dynamic voltage increases the response amplitude when it is increased. An analogy between Fig. 7 and Fig. 8, one can conclude that the influence of the DC voltage is more than the AC voltage amplitude.

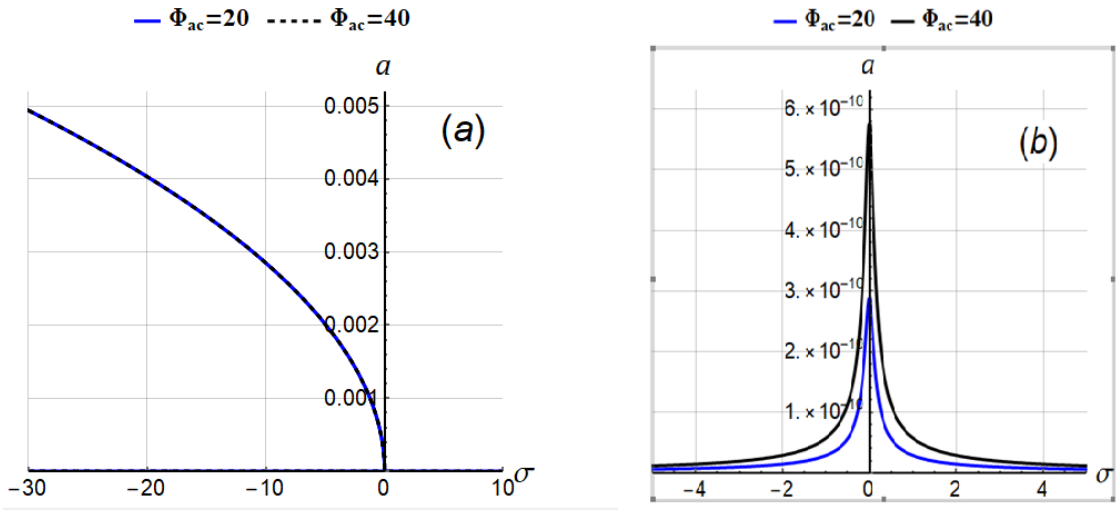

Figure. 8. Influence of AC voltage Φ_{ac} on the Frequency amplitude curve of the dielectric elastomer-based microcantilever atomic force microscope probe. (a) $\bar{C} = 0$, (b) $\bar{C} = 0.1$.

The classical continuum mechanics models cannot accurately predict mechanical structures' response on micro/nanoscale. For this reason, size-dependent models are utilized to overcome this drawback. As discussed in the mathematical modeling, we have employed the modified couple stress theory in the current research. The difference between the classical theory and the modified couple stress theory is the presence of the parameter ℓ. Here, we examine the influence of ℓ on the structure's frequency response in Fig. 9. From this figure, we conclude that the influence of the size on the system with and without damping is very different. For undamped AFM, the size decreases the softening nonlinearity when it is increased, and also it increases the response amplitude. But, for the damped AFM, increasing the size effects decrease the response amplitude.

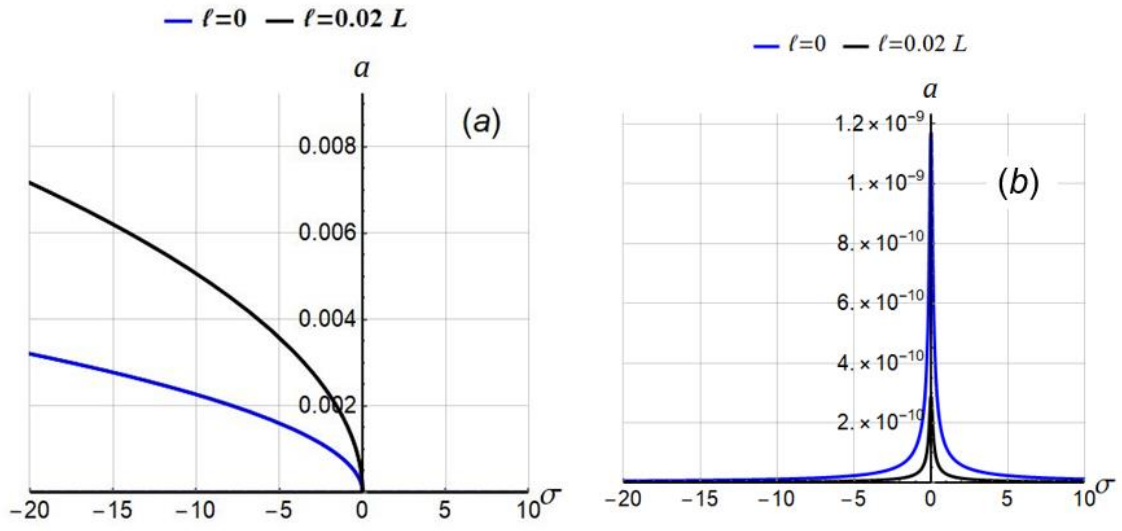

Figure. 9. Influence of size-effect parameter ℓ on the Frequency amplitude curve of the dielectric elastomer-based microcantilever atomic force microscope probe. (a) $\bar{C} = 0$, (b) $\bar{C} = 0.1$

Previous numerical simulations were for the forced vibration in the frequency domain, which is obtained and described by means of the analytical solutions of the equation of motion. In what follows, the forced vibration is investigated in the time domain by numerically solving of Eq. (42).

We generate Fig. 10 to identify the overall trend of the forced vibration of the DE-based AFM. the DE-based AFM under $\Phi_{dc} = 100$Volt, $\Phi_{ac} = 20$, and $\Omega = 5$, wherein a non-damped condition is assumed, i.e., $c = 0$, and the initial transverse motion is $W(0) = 0.0001$. The plot of velocity versus displacement of the coordinate system originated from the non-transient of the time history, leading to the phase-plane diagram. To conduct signal processing (FFT), continuous signals in the time history are discretized using the FFT scheme. In order to avoid aliasing, a large enough sample rate is adopted for the FFT. Looking at this figure, it is apparent that the DE-based AFM encounters a quasiperiodic dynamic response. This trend is better interpreted in the Poincaré map, in which a closed loop of points appears, showing quasiperiodicity. Narrowband and distinguished spectra in FFT prove the quasiperiodicity of response.

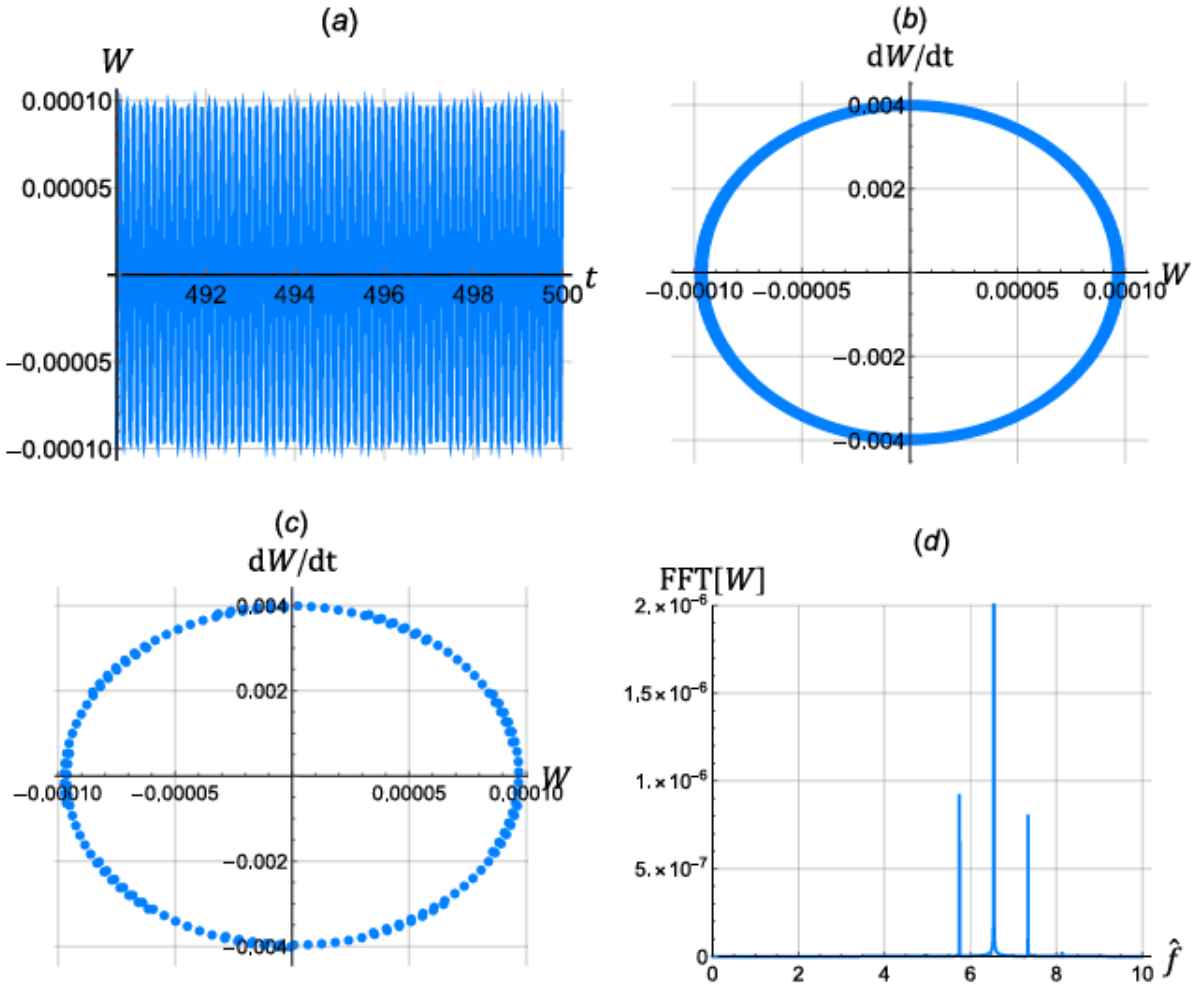

Figure 10. Dynamic characteristics of the dielectric elastomer-based microcantilever atomic force microscope probe under $\Phi_{dc} = 100$Volt, $\Phi_{ac} = 20$, $\Omega = 5$, and $c = 0$ with $W(0) = 0.0001$ and $\dot{W}(0) = 0$. (a) time history, (b) phase-plane diagram, (c) Poincaré map, (d) FFT.

As stated before, the DE-based AFM is mathematically nonlinear and named a nonlinear system. It is well-known that an essential characteristic of such systems is their sensitivity to initial conditions. It means that a minor change in initial conditions may vigorously complicate the response of nonlinear systems. For this purpose, in Fig. 11, we assess the influence of the initial condition on the forced vibration of the considered system. The system's parameters and the traverse motion rate $\dot{W}$ are the same as those used in Fig. 10, but we choose two initial conditions, i.e., $W(0) = 0.0004980$ and 0.0004982. Inspecting the figure, one quickly sees that increasing the initial transverse displacement leads to instability in the system. But, it is difficult to exactly say this instability is due to the numerical integration or the instability in real applications that the system may fail and be destroyed.

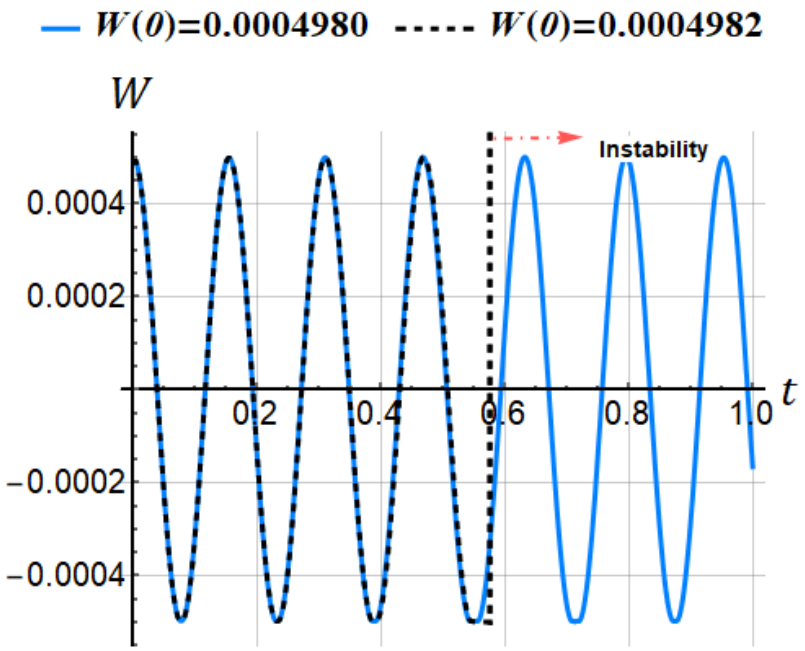

Figure 11. Influence of the initial conditions on the dynamic characteristics of the dielectric elastomer-based microcantilever atomic force microscope probe under $\Phi_{dc} = 100\text{Volt}$, $\Phi_{ac} = 20$, $\Omega = 5$, and $c = 0$.

7. Verification study

In order to evaluate the accuracy of our model, a verification process is carried out. A comparison is made between this paper and the reference. To this end, parameters in reference [42] are utilized, such that $L = 225\mu\text{m}, I = 3.57 \times 10^{-23}\text{m}^4$, $A = 7.2 \times 10^{-11}\text{m}^2$, $H = 2.96 \times 10^{-19}\text{J}$, $R = 10\text{nm}$, $E = 170\text{GPa}$. Terms relation to the voltage, length-scale parameter, and cubic term in Eq. (16) is equal to zero. In Fig. 12, equilibrium tip/sample separation Δ is plotted versus different initial tip/sample separation Z. It is seen that good agreement between this paper and reference [42] is obtained.

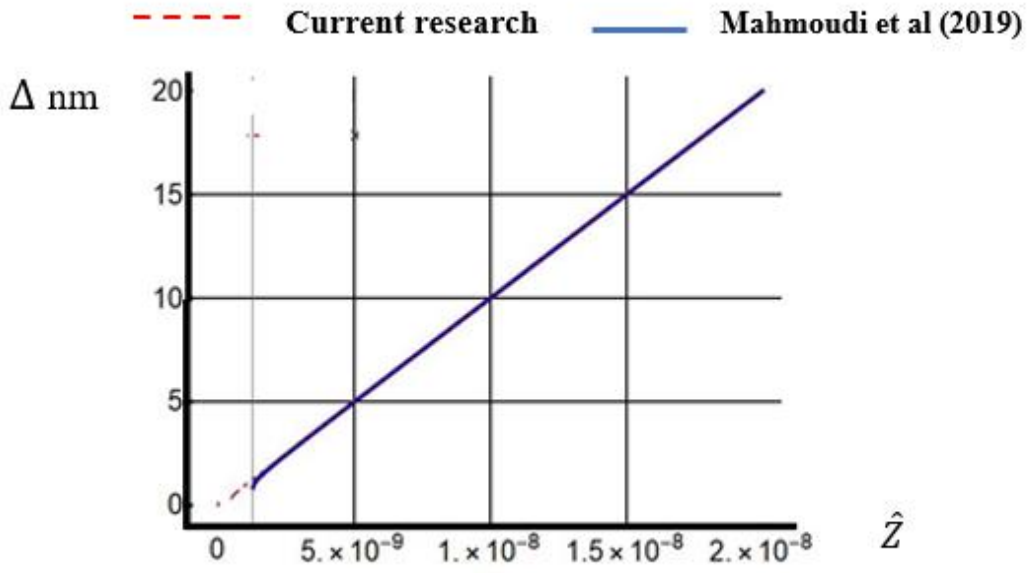

Figure. 12. Static response of the system. Comparison between this paper and reference [42].

8. Perspective and challenge for AFM based on DEs

Previous studies have reported that DEs can operate in different environments such as water, air, and vacuum. In real-world applications, some parameters may notably affect the response of DE, for instance, temperature and moisture. Thus, if AFM, excited by DE actuators, works in water or air, these factors should be taken into account. It is noted that DEs have good performance in such environments. As an example, it has been shown that DEs can work well in water. As reported, the absorption of water by DEs is very little. Therefore, water may not change significantly the performance and properties of DEs, for example, their viscosity [56]. Another important factor in the real application is the gas damping that may affect the quality factor of the DE-based microcantilever. Nonetheless, if the ambient pressure is as low as 10^{-6} atm, the gas damping may be omitted. This assumption has been considered in this paper.

A high voltage actuation may lead to collapse. But, as mentioned in the experimental and theoretical studies, the dielectric elastomer can undergo high voltage even for some structures in the kilovolt range. This paper theoretically presents a value of 100 V for the voltage, and it is seen that the AFM can operate without collapse. However, the dielectric elastomer may operate even at lower voltages if an appropriate material for electrodes is fabricated. Although one of the initial limitations of DE has been the need for high-voltage, it has been overcome by fabrications of novel electrodes.

The microcantilever used in this paper is designed as a DE, i.e., the whole body of the cantilever consists of a DE. Another discussion raised is that DEs can operate such as piezoelectric patches to vibrate any microcantilever, even those with rigid elastic constant. This would be our future aim to analyze the possibility of such a mechanism for AFM.

9. Conclusions

In this work, a dielectric elastomer actuator was proposed to drive microcantilevers in atomic force microscopy. More specifically, dynamic modeling of dielectric elastomer-based atomic force

microscopy was implemented. A hyperelastic micropolar model that includes moderate rotation, large deformation, and size effects was employed as the constative material model for the dielectric elastomer. The elastomer was assumed to be incompressible, and its damping attribute was also incorporated. Free and forced vibrations equations of motion are derived via Hamilton's principle and solved with the aid of a Gear implicit backward differentiation scheme and multiple time-scales method. The results of the present research are listed below.

- A periodic motion is seen for the static voltage loading of the system.
- There is evidence that the DE-AFM driven by a sinusoidal voltage leads to quasiperiodic vibrations.
- With the contribution of the damping force to the system, a decreasing trend of the response amplitude is found.
- The resonance of the system is softening type.
- With the increase of the size-effect parameter, the softening nonlinearity gets weaker when damping is neglected.
- For the damped DE-based AFM, the response amplitude gets lowered with the increase of the size-effect parameter.
- A change in DC and AC voltages can tune the resonant regions of the AFM.

This paper is a theoretical analysis merely, and we hope that future empirical tests will confirm the results and model proposed here.

Supplementary Materials:
Author Contributions: "Conceptualization, A.A. and Sh.D.; methodology, A.A.; software, A.A.; validation, A.A. and Sh.D.; formal analysis, A.A.; investigation, M.M and V.E.; resources, A.A. and M.M.; data curation, A.A.; writing—original draft preparation, A.A. and Sh.D.; writing—review and editing, A.A., Sh.D., M.M., and V.E.; visualization, A.A., Sh.D.; supervision, V.E.; project administration, M.M., and V.E.; funding acquisition, Sh.D., and M.M.. All authors have read and agreed to the published version of the manuscript.

Funding: This research received no external funding.
Data Availability Statement: Data sharing not applicable.
Conflicts of Interest: The authors declare no conflict of interest.

References

1. Kim, I.J., Cho, K.Y., Kim, E., Kwon, Y.J., Shon, M.Y., Park, B.I., Yu, S., Lee, J.H.: Development of High Dielectric Electrostrictive PVDF Terpolymer Blends for Enhanced Electromechanical Properties. Nanomater. 2021, Vol. 11, Page 6. 11, 6 (2020). https://doi.org/10.3390/NANO11010006
2. Moretti, G., Rosset, S., Vertechy, R., Anderson, I., Fontana, M.: A Review of Dielectric Elastomer Generator Systems. Adv. Intell. Syst. 2, (2020). https://doi.org/10.1002/aisy.202070103
3. Lu, T., Ma, C., Wang, T.: Mechanics of dielectric elastomer structures: A review. Extrem. Mech. Lett. 38, (2020). https://doi.org/10.1016/j.eml.2020.100752
4. D'anniballe, R., Zucchelli, A., Carloni, R.: Towards Poly(vinylidene fluoride-trifluoroethylene-chlorotrifluoroethylene)-Based Soft Actuators: Films and Electrospun Aligned Nanofiber Mats. Nanomater. 2021, Vol. 11, Page 172. 11, 172 (2021). https://doi.org/10.3390/NANO11010172
5. Boyraz, P., Runge, G., Raatz, A.: An overview of novel actuators for soft robotics, (2018)
6. Youn, J.H., Jeong, S.M., Hwang, G., Kim, H., Hyeon, K., Park, J., Kyung, K.U.: Dielectric

elastomer actuator for soft robotics applications and challenges. Appl. Sci. 10, (2020). https://doi.org/10.3390/app10020640
7. Thomson, G., Lai, Z., Val, D. V., Yurchenko, D.: Advantages of nonlinear energy harvesting with dielectric elastomers. J. Sound Vib. 442, (2019). https://doi.org/10.1016/j.jsv.2018.10.066
8. Liu, L., Ma, W., Chen, H.L., Li, B.: Oscillation of Dielectric Elastomers Resonator with Strain-Stiffening Effect. In: 9th IEEE International Conference on Cyber Technology in Automation, Control and Intelligent Systems, CYBER 2019 (2019)
9. Ariana, A., Mohammadi, A.K.: Nonlinear dynamics and bifurcation behavior of a sandwiched micro-beam resonator consist of hyper-elastic dielectric film. Sensors Actuators, A Phys. 312, (2020). https://doi.org/10.1016/j.sna.2020.112113
10. Zhu, J., Cai, S., Suo, Z.: Nonlinear oscillation of a dielectric elastomer balloon. Polym. Int. 59, 378–383 (2010). https://doi.org/10.1002/PI.2767
11. Jin, X., Huang, Z.: Random response of dielectric elastomer balloon to electrical or mechanical perturbation. J. Intell. Mater. Syst. Struct. 28, (2017). https://doi.org/10.1177/1045389X16649446
12. Sharma, A.K., Arora, N., Joglekar, M.M.: DC dynamic pull-in instability of a dielectric elastomer balloon: An energy-based approach. In: Proceedings of the Royal Society A: Mathematical, Physical and Engineering Sciences (2018)
13. Wang, F., Lu, T., Wang, T.J.: Nonlinear vibration of dielectric elastomer incorporating strain stiffening. Int. J. Solids Struct. 87, (2016). https://doi.org/10.1016/j.ijsolstr.2016.02.030
14. Alibakhshi, A., Heidari, H.: Analytical approximation solutions of a dielectric elastomer balloon using the multiple scales method. Eur. J. Mech. A/Solids. 74, (2019). https://doi.org/10.1016/j.euromechsol.2019.01.009
15. Alibakhshi, A., Heidari, H.: Nonlinear dynamics of dielectric elastomer balloons based on the Gent-Gent hyperelastic model. Eur. J. Mech. A/Solids. 82, (2020). https://doi.org/10.1016/j.euromechsol.2020.103986
16. Zhang, J., Chen, H.: Voltage-induced beating vibration of a dielectric elastomer membrane. Nonlinear Dyn. 100, (2020). https://doi.org/10.1007/s11071-020-05678-4
17. Heidari, H., Alibakhshi, A., Azarboni, H.R.: Chaotic Motion of a Parametrically Excited Dielectric Elastomer. Int. J. Appl. Mech. 12, (2020). https://doi.org/10.1142/S1758825120500337
18. Alibakhshi, A., Imam, A., Haghighi, S.E.: Effect of the second invariant of the Cauchy–Green deformation tensor on the local dynamics of dielectric elastomers. Int. J. Non. Linear. Mech. 137, (2021). https://doi.org/10.1016/j.ijnonlinmec.2021.103807
19. Feng, C., Jiang, L., Lau, W.M.: Dynamic characteristics of a dielectric elastomer-based microbeam resonator with small vibration amplitude. J. Micromechanics Microengineering. 21, (2011). https://doi.org/10.1088/0960-1317/21/9/095002
20. Feng, C., Yu, L., Zhang, W.: Dynamic analysis of a dielectric elastomer-based microbeam resonator with large vibration amplitude. Int. J. Non. Linear. Mech. 65, (2014). https://doi.org/10.1016/j.ijnonlinmec.2014.05.004
21. Alibakhshi, A., Heidari, H.: Nonlinear dynamic responses of electrically actuated dielectric elastomer-based microbeam resonators. J. Intell. Mater. Syst. Struct. (2021). https://doi.org/10.1177/1045389x211023584
22. Dastjerdi, S., Abbasi, M.: A vibration analysis of a cracked micro-cantilever in an atomic force microscope by using transfer matrix method. Ultramicroscopy. 196, (2019). https://doi.org/10.1016/j.ultramic.2018.09.014
23. Arafat, H.N., Nayfeh, A.H., Abdel-Rahman, E.M.: Modal interactions in contact-mode atomic force microscopes. Nonlinear Dyn. 54, (2008). https://doi.org/10.1007/s11071-008-9388-5
24. Sader, J.E., Chon, J.W.M., Mulvaney, P.: Calibration of rectangular atomic force microscope cantilevers. Rev. Sci. Instrum. 70, (1999). https://doi.org/10.1063/1.1150021
25. Long, C.J., Cannara, R.J.: Modular apparatus for electrostatic actuation of common atomic force microscope cantilevers. Rev. Sci. Instrum. 86, (2015). https://doi.org/10.1063/1.4926431
26. Degertekin, F.L.: Novel atomic force microscope probes with integrated electrostatic actuation and

optical detection. In: Conference Proceedings - Lasers and Electro-Optics Society Annual Meeting-LEOS (2007)
27. Zhang, G., Gaspar, J., Chu, V., Conde, J.P.: Electrostatically actuated polymer microresonators. Appl. Phys. Lett. 87, (2005). https://doi.org/10.1063/1.2040009
28. Şimşek, M., Reddy, J.N.: Bending and vibration of functionally graded microbeams using a new higher order beam theory and the modified couple stress theory. Int. J. Eng. Sci. 64, (2013). https://doi.org/10.1016/j.ijengsci.2012.12.002
29. Vaccaro, M.S., Pinnola, F.P., de Sciarra, F.M., Barretta, R.: Elastostatics of bernoulli–euler beams resting on displacement-driven nonlocal foundation. Nanomaterials. 11, (2021). https://doi.org/10.3390/nano11030573
30. Avcar, M., Hadji, L., Civalek, Ö.: Natural frequency analysis of sigmoid functionally graded sandwich beams in the framework of high order shear deformation theory. Compos. Struct. 276, (2021). https://doi.org/10.1016/j.compstruct.2021.114564
31. Hadji, L., Avcar, M.: Nonlocal free vibration analysis of porous FG nanobeams using hyperbolic shear deformation beam theory. Adv. Nano Res. 10, (2021). https://doi.org/10.12989/anr.2021.10.3.281
32. Avcar, M.: Free vibration of imperfect sigmoid and power law functionally graded beams. Steel Compos. Struct. 30, (2019). https://doi.org/10.12989/scs.2019.30.6.603
33. Hadji, L., Avcar, M., Civalek, Ö.: An analytical solution for the free vibration of FG nanoplates. J. Brazilian Soc. Mech. Sci. Eng. 43, (2021). https://doi.org/10.1007/s40430-021-03134-x
34. Lu, L., She, G. L., Guo, X.: Size-dependent postbuckling analysis of graphene reinforced composite microtubes with geometrical imperfection. Int. J. Mech. Sci. 199, (2021). https://doi.org/10.1016/j.ijmecsci.2021.106428
35. Malikan, M., Eremeyev, V. A.: A new hyperbolic-polynomial higher-order elasticity theory for mechanics of thick FGM beams with imperfection in the material composition. Compos. Struct. 249, (2020). https://doi.org/10.1016/j.compstruct.2020.112486
36. Amabili, M.: Nonlinear vibrations and stability of shells and plates. (2008)
37. Srinivasa, A.R., Reddy, J.N.: A model for a constrained, finitely deforming, elastic solid with rotation gradient dependent strain energy, and its specialization to von Kármán plates and beams. J. Mech. Phys. Solids. 61, (2013). https://doi.org/10.1016/j.jmps.2012.10.008
38. Alibakhshi, A., Dastjerdi, S., Akgöz, B., Civalek, Ö.: Parametric Vibration of a Dielectric Elastomer Microbeam Resonator Based on a Hyperelastic Cosserat Continuum Model. Compos. Struct. 115386 (2022). https://doi.org/10.1016/J.COMPSTRUCT.2022.115386
39. Amabili, M.: Nonlinear Mechanics of Shells and Plates in Composite, Soft and Biological Materials. (2018)
40. Reddy, J.N., Srinivasa, A.R.: Non-linear theories of beams and plates accounting for moderate rotations and material length scales. Int. J. Non. Linear. Mech. 66, (2014). https://doi.org/10.1016/j.ijnonlinmec.2014.06.003
41. Bahrami, A., Nayfeh, A.H.: On the dynamics of tapping mode atomic force microscope probes. Nonlinear Dyn. 70, (2012). https://doi.org/10.1007/s11071-012-0560-6
42. Mahmoudi, M.S., Ebrahimian, A., Bahrami, A.: Higher modes and higher harmonics in the non-contact atomic force microscopy. Int. J. Non. Linear. Mech. 110, (2019). https://doi.org/10.1016/j.ijnonlinmec.2019.01.006
43. Ghayesh, M.H., Farokhi, H., Amabili, M.: Nonlinear behaviour of electrically actuated MEMS resonators. Int. J. Eng. Sci. 71, (2013). https://doi.org/10.1016/j.ijengsci.2013.05.006
44. Civalek, Ö., Akbaş, Ş.D., Akgöz, B., Dastjerdi, S.: Forced vibration analysis of composite beams reinforced by carbon nanotubes. Nanomaterials. 11, (2021). https://doi.org/10.3390/nano11030571
45. Liu, Y.F., Wang, Y.Q.: Thermo-electro-mechanical vibrations of porous functionally graded piezoelectric nanoshells. Nanomaterials. 9, (2019). https://doi.org/10.3390/nano9020301
46. Dastjerdi, S., Malikan, M., Dimitri, R., Tornabene, F.: Nonlocal elasticity analysis of moderately thick porous functionally graded plates in a hygro-thermal environment. Compos. Struct. 255,

(2021). https://doi.org/10.1016/j.compstruct.2020.112925
47. Dastjerdi, S., Akgöz, B., Civalek, Ö.: On the effect of viscoelasticity on behavior of gyroscopes. Int. J. Eng. Sci. 149, (2020). https://doi.org/10.1016/j.ijengsci.2020.103236
48. Alibakhshi, A., Dastjerdi, S., Malikan, M., Eremeyev, V.A.: Nonlinear Free and Forced Vibrations of a Hyperelastic Micro/Nanobeam Considering Strain Stiffening Effect. Nanomater. 2021, Vol. 11, Page 3066. 11, 3066 (2021). https://doi.org/10.3390/NANO11113066
49. Malikan, M., Dimitri, R., Tornabene, F.: Transient response of oscillated carbon nanotubes with an internal and external damping. Compos. Part B Eng. 158, (2019). https://doi.org/10.1016/j.compositesb.2018.09.092
50. Malikan, M., Eremeyev, V.A.: Flexomagnetic response of buckled piezomagnetic composite nanoplates. Compos. Struct. 267, (2021). https://doi.org/10.1016/j.compstruct.2021.113932
51. Aranda-Ruiz, J., Fernández-Sáez, J.: On the use of variable-separation method for the analysis of vibration problems with time-dependent boundary conditions. Proc. Inst. Mech. Eng. Part C J. Mech. Eng. Sci. 226, (2012). https://doi.org/10.1177/0954406212442289
52. Younis, M.I.: MEMS Linear and Nonlinear Statics and Dynamics. (2011)
53. Ali Hasan Nayfeh: Introduction to perturbation techniques. John Wiley & Sons (2011)
54. Fathalilou, M., Rezaei-Abajelou, P., Vefaghi, A., Rezazadeh, G.: Dielectric Elastomer as a New Material for Electrostatically Actuated Microbeams: Stability Analysis. Int. J. Appl. Mech. 11, (2019). https://doi.org/10.1142/S1758825119500984
55. Azarboni, H.R., Rahimzadeh, M., Heidari, H., Keshavarzpour, H., Edalatpanah, S.A.: Chaotic dynamics and primary resonance analysis of a curved carbon nanotube considering influence of thermal and magnetic fields. J. Brazilian Soc. Mech. Sci. Eng. 41, (2019). https://doi.org/10.1007/s40430-019-1795-7
56. Shintake, J., Cacucciolo, V., Shea, H., Floreano, D.: Soft biomimetic fish robot made of dielectric elastomer actuators. Soft Robot. 5, (2018). https://doi.org/10.1089/soro.2017.0062